

Atomistic modeling of extreme near-field heat transport across nanogaps between two polar dielectric materials

Yangyu Guo^{1,3,*}, Mauricio Gómez Vitoria², Riccardo Messina², Philippe Ben-Abdallah², and Samy Merabia^{3,†}

¹*School of Energy Science and Engineering, Harbin Institute of Technology, Harbin 150001, China*

²*Laboratoire Charles Fabry, UMR 8501, Institut d'Optique, CNRS, Université Paris-Saclay, 2, Avenue Augustin Fresnel, 91127 Palaiseau Cedex, France*

³*Institut Lumière Matière, Université Claude Bernard Lyon 1-CNRS, Université de Lyon, Villeurbanne 69622, France*



(Received 22 May 2023; revised 17 August 2023; accepted 21 August 2023; published 29 August 2023)

The understanding of extreme near-field heat transport across vacuum nanogaps between polar dielectric materials remains an open question. In this work, we present an investigation of heat transport across vacuum nanogaps between magnesium oxide (MgO) surfaces by nonequilibrium molecular dynamics (NEMD) simulation, which naturally accounts for the nonlocal dielectric response from both acoustic and optical branches as well as phonon tunneling. A consistent comparison is also made with the continuum fluctuational electrodynamics theory using both local and nonlocal dielectric functions computed by equilibrium molecular dynamics with the anharmonic damping properly included. As a result, the direct NEMD result shows significant deviations from the continuum theory even up to a gap size of a few nanometers. The lattice anharmonicity is demonstrated to have a large impact on the energy transmission and thermal conductance, in contrast to its moderate effect reported for metallic vacuum nanogaps. The present work thus provides further insight into the physics of heat transport in the extreme near-field regime between polar materials, and puts forward a methodology to account for anharmonic effects.

DOI: [10.1103/PhysRevB.108.085434](https://doi.org/10.1103/PhysRevB.108.085434)

I. INTRODUCTION

When the gap between two objects is smaller than the thermal wavelength of photons ($\sim 10 \mu\text{m}$ at 300 K), the radiative heat transfer enters the near-field regime, where the heat flux can be several orders of magnitude higher than that predicted by the Stefan-Boltzmann law [1,2]. The near-field radiative heat transfer (NFRHT) has been well described by the classical fluctuational electrodynamics (FE) theory [3], as widely verified by numerous experiments during the past decades [4–14]. However, it remains still an open question to fully understand the physics which drives the heat exchanges in the extreme near-field regime, when the separation gap becomes smaller than a few nanometers, corresponding to the transition regime between radiation and conduction. There have been very few experimental studies in such a regime [15–19]. Those works were mainly limited to the study of heat transfer between metals and they yielded conflicting conclusions about the validity of the classical FE theory at gap size below a few nanometers [11,17,18].

The investigation of extreme near-field heat transport is of vital significance in many applications such as near-field scanning thermal microscopy [20–22], heat-assisted magnetic recording [23–25], nanophotolithography [26], or noncontact friction [27,28]. On the other hand, it is of fundamental

interest due to the emerging novel physics at such small scale including (i) the tunneling of phonons [29–32] and electrons [33–35] across a vacuum nanogap, and (ii) the nonlocal dielectric response of materials [36,37]. Very recently, the role played by the acoustic phonon modes in the nonlocal dielectric response of polar materials has been highlighted and its importance on the heat transfer close to the contact has been demonstrated [37]. Atomistic modeling becomes an essential tool to uncover the underlying physics in the extreme near-field regime, and also provide a reference to examine the validity of the continuum FE theory. The contribution of phonon tunneling across vacuum nanogaps between two infinite metallic plates has been studied by atomistic methods [38–41]. Similar atomistic studies have been conducted on heat transport across Si nanogaps using either empirical potential [42] or first-principles calculations [43]. Those works showed that the phonon thermal conductance decays very rapidly as the gap size increases due to the relatively short range of atomic interactions in metallic and apolar solid systems. Generally the contribution of phonon tunneling becomes negligible beyond a gap size of 1 nm, beyond which the photonic contribution dominates [41,43]. Yet, very few studies have considered heat transfer across nanogaps between polar materials from an atomistic point of view.

In this work, we focus our attention on the extreme near-field heat transport between polar materials across vacuum gaps much thinner than the range of atomic interactions. A molecular dynamics (MD) simulation of heat transport between two silica nanoparticles was shown [44] to agree with the dipole-dipole interaction model after a separation distance

*yyguo@hit.edu.cn

†samy.merabia@univ-lyon1.fr

of a few diameters, where the thermal conductance (h) decays with the gap size (d) as $h \propto d^{-6}$. Such power law was later obtained by a harmonic nonequilibrium Green's function (NEGF) simulation of the same configuration [45], where a slower decay of thermal conductance $h \propto d^{-4}$ was further shown at smaller gap size between 4 Å and a few diameters due to the surface charge-charge interaction. The electron-cloud overlap and transition to heat conduction was finally inferred below a gap size of 4 Å [45]. Recently, the transition from NFRHT to heat conduction was also studied across a vacuum gap between two infinite sodium chloride (NaCl) plates [46] by coupling the Maxwell equations to harmonic NEGF simulation. The thermal conductance across the gap predicted by the NEGF has been demonstrated to recover that by the FE theory beyond a gap size of ~ 1 nm, below which appreciable deviation was observed [46]. However, the long-range Coulomb interaction forces as input into NEGF were obtained from the solution of Maxwell equations for a system of harmonically oscillating charged ions. The role of lattice anharmonicity is still elusive in their comparison of harmonic NEGF with FE theory, the latter requiring the dielectric function including the anharmonic damping. Thus, the critical gap size below which the classical FE theory becomes invalid remains today an open question for extreme near-field heat transport between polar dielectrics [14].

Therefore, the current work aims to present a nonequilibrium molecular dynamics (NEMD) simulation of extreme near-field heat transport across a vacuum nanogap between two infinite MgO plates. A more realistic description of the anharmonic dynamics of ions and their long-range Coulomb interaction is provided in MD using an empirical potential [47], which describes reasonably well the dielectric function of the material. Furthermore, we propose a more consistent comparison between the direct NEMD and FE theory by supplementing the latter with local dielectric function calculated from equilibrium molecular dynamics (EMD). As a result, we demonstrate a non-negligible deviation of NEMD from FE theory up to a gap size of 2 nm, while a gradual recovery of FE theory is expected at larger gap. This will provide a more reasonable examination of the validity of FE theory in radiative heat transfer across vacuum nanogaps between polar dielectric materials. Finally, the role of anharmonicity, which is naturally included in NEMD, is shown to have appreciable effect on the energy transmission across the nanogap. The remaining of this paper is organized as follows: The methodology of atomistic modeling will be introduced in Sec. II, followed by a discussion of the results in Sec. III, and the concluding remarks will be made in Sec. IV.

II. METHODOLOGY

In this section, we first introduce in Sec. II A the NEMD model of the MgO-MgO vacuum nanogap. The method to extract the spectral thermal conductance for the comparison with FE theory is also explained. In Sec. II B, we present a summary of FE theory for NFRHT between two infinite plates, together with the EMD method to calculate the local dielectric function as input.

TABLE I. Parameters in empirical potential Eq. (1) for MgO.

Atom	e (Elementary charge)	A (Å)	B (Å)	C (Å ³ kJ ^{1/2} mol ^{-1/2})
Mg	+1.40	1.0133	0.052	0
O	-1.40	1.8020	0.150	54

A. NEMD simulation and analysis

Heat transport across a parallel vacuum MgO-MgO nanogap is simulated by NEMD as implemented in the open-source package LAMMPS [48], as shown in Fig. 1. The nanogap is obtained by shifting half part of a bulk MgO crystal along the [1 0 0] direction. In NEMD, the nanogap is sandwiched between a hot thermostat and a cold thermostat, with two fixed-layer regions at both ends. These fixed layers will not be involved in the evolution of the atomic dynamics during the steady-state run, and are used to avoid the macroscopic drift of the system, i.e., ensure its stability. Periodic boundary conditions are imposed along the three directions of the system. The following pairwise atomic interaction potential is employed [47]:

$$\phi_{ij} = \frac{e_i e_j}{r_{ij}} - \frac{C_i C_j}{r_{ij}^6} + f(B_i + B_j) \exp\left(\frac{A_i + A_j - r_{ij}}{B_i + B_j}\right), \quad (1)$$

where the distance between atom i and atom j is $r_{ij} = |\mathbf{r}_i - \mathbf{r}_j|$, $e_{i(j)}$ is the effective charge of atom $i(j)$, and $f = 4.184$ kJ/Å/mol, with other atomic parameters $A_{i(j)}$, $B_{i(j)}$, and $C_{i(j)}$ given in Table I [47]. Such a potential includes both long-range Coulomb interaction (the first term) and short-range bonding interaction (the second and third terms). This potential is adopted as it reproduces well the dielectric response of bulk MgO in the infrared regime [49], which is crucial for accurately describing the near-field heat transport across a vacuum gap [44]. The particle-particle particle-mesh method [50] is implemented for the treatment of long-range Coulomb force with a cutoff radius of 10 Å for the direct interactions in real space.

Four gap sizes from 6 Å to 2 nm are considered, and the detailed dimensions of the NEMD model after careful size-independence verification are provided in Table II. The length of the fixed-layer region (L_f) should be sufficiently large to avoid direct long-range interaction between the thermostats through the periodic boundary condition in the transport direction. In addition, the length of the device region on one side of the nanogap (L_d) should be sufficiently large to avoid direct long-range interaction between the thermostat on this side and the device region on the other side. A more

TABLE II. Dimension (in u.c., i.e., conventional unit cell of MgO) of NEMD model of MgO-MgO nanogap shown in Fig. 1.

Gap size d (nm)	L_f (u.c.)	L_{th} (u.c.)	L_d (u.c.)	Cross section (u.c. \times u.c.)
0.6	8	5	8	8×8
1.0	12	5	12	8×8
1.2	12	5	12	8×8
2.0	14	5	14	10×10

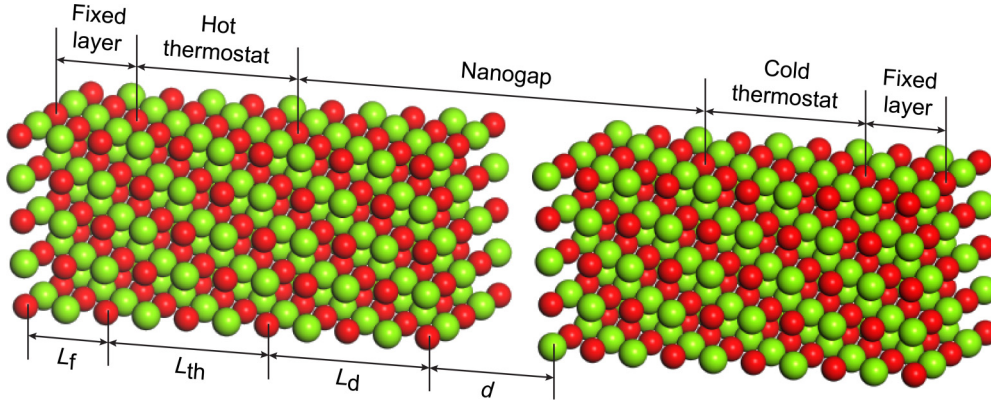


FIG. 1. Schematic of NEMD model of MgO-MgO nanogap with gap size d . Red and green atoms denote Mg^{2+} and O^{2-} ions, respectively. Lengths of fixed layer and thermostat are L_f and L_{th} , respectively, whereas length of device region on one side of nanogap is L_d . System is symmetric in terms of size. Periodic boundary conditions are applied along three directions of system.

detailed description of the size-independence verification is given in Appendix. The sufficiently thick fixed-layer and device regions make the vacuum gap feel as if there are two semi-infinite contacts, which minimizes the effect of fictitious cross-gap forces from periodic images along the transport direction. During the NEMD simulation, a time step of 0.5 fs is adopted. First, 1×10^6 time steps are run to relax the whole system under the *NPT* (isothermal-isobaric) ensemble. Then, the fixed-layer regions are fixed and 2×10^6 time steps are run to make the remaining free part reach a steady state under the effect of Langevin thermostats in the *NVE* (microcanonical) ensemble. Finally, 4×10^6 time steps of steady-state runs are performed for the calculation of the spectral and the overall thermal conductance of the nanogap. Five independent NEMD simulations are conducted for each gap size to reduce the statistical fluctuations.

The total heat flow from one side (I) of the nanogap device region to the other side (J) can be decomposed into its spectral component as

$$Q_{I \rightarrow J} = \int_0^\infty q(\omega) \frac{d\omega}{2\pi}, \quad (2)$$

with ω the angular frequency and the spectral (i.e., frequency-dependent) heat flow computed from the Fourier transform of the time (t) correlation function between atomic force and velocity [51,52]:

$$q(\omega) = 2\text{Re} \sum_{\substack{i \in I \\ j \in J}} \int_{-\infty}^{\infty} \langle \mathbf{F}_{ji}(t) \cdot \mathbf{v}_j(0) \rangle \exp(i\omega t) dt, \quad (3)$$

where Re denotes the real part, \mathbf{F}_{ji} denotes the force on atom j due to atom i , with \mathbf{v}_j the atomic velocity, and the bracket $\langle \rangle$ represents the nonequilibrium ensemble average as calculated by time average. Equation (3) essentially gives the magnitude of heat flow as a sum of the net power exchange ($\mathbf{F}_{ji} \cdot \mathbf{v}_j - \mathbf{F}_{ij} \cdot \mathbf{v}_i$, as a microscopic quantity) between individual atomic pairs [44,51]. The direction of heat flow (as a macroscopic quantity) is determined as the direction from the center of one region (I) to that of the other region (J). Following a previous study [53], we slightly transform Eq. (3) into the following

form to avoid the huge storage of all the interatomic forces:

$$q(\omega) = 2\text{Re} \sum_{j \in J} \int_{-\infty}^{\infty} \langle \mathbf{F}_j(t) \cdot \mathbf{v}_j(0) \rangle \exp(i\omega t) dt, \quad (4)$$

with $\mathbf{F}_j(t) = \sum_{i \in I} \mathbf{F}_{ji}(t)$ the overall force on atom j in region J from all the atoms in region I . It has been assumed that the ensemble average and the sum over I are interchangeable. Such an assumption is valid since the ensemble average is calculated by time average, as also verified in previous studies [53,54].

With the spectral heat flow obtained from NEMD simulation via Eq. (4), the transmission function across the nanogap is computed as [51]

$$\Xi(\omega) = \frac{q(\omega)}{k_B \Delta T}, \quad (5)$$

where k_B is the Boltzmann constant, and ΔT is the temperature difference between the hot and cold thermostats. The transmission function represents the product of the number of available modes at a specific frequency and their transmittance (≤ 1) [55]. Based on Landauer's formula, the classical and quantum thermal conductances per unit area of the nanogap can be computed, respectively, by [41]

$$h_{\text{classical}} = \frac{1}{A_c} \int_0^\infty k_B \Xi(\omega) \frac{d\omega}{2\pi}, \quad (6)$$

$$h_{\text{quantum}} = \frac{1}{A_c} \int_0^\infty \hbar \omega \frac{\partial f_{\text{BE}}(\omega)}{\partial T} \Xi(\omega) \frac{d\omega}{2\pi}. \quad (7)$$

In Eq. (6) and Eq. (7), the classical (k_B) and quantum heat capacity [$\hbar \omega \partial f_{\text{BE}}(\omega) / \partial T$] are used, respectively, with \hbar the reduced Planck constant, $f_{\text{BE}}(\omega)$ the Bose-Einstein equilibrium distribution, and A_c the cross-section area of the nanogap.

B. Fluctuational electrodynamics theory with EMD inputs

In parallel, we will compare the NEMD result to the prediction of FE theory using inputs of local dielectric function from EMD (denoted as FE local theory). The NFRHT has been well described by the FE theory, which predicts the net heat flux between two infinite parallel plates at T_1 and T_2 , respectively,

as [2,56]

$$\Phi = \frac{1}{4\pi^2} \int_0^\infty \int_0^\infty [\Theta(\omega, T_1) - \Theta(\omega, T_2)] \times \xi_{12}(\omega, k_{\parallel}) k_{\parallel} dk_{\parallel} d\omega, \quad (8)$$

where $\Theta(\omega, T) = \hbar\omega[f_{\text{BE}}(\omega, T) + 1/2]$ is the mean energy of Planck oscillator at equilibrium with 1/2 accounting for the vacuum fluctuations or zero-point energy, and k_{\parallel} is the parallel component of the photon wave vector, whereas $\xi_{12}(\omega, k_{\parallel})$ is the photon tunneling probability. In the limit of small temperature difference, Eq. (8) can be rewritten into the form of Landauer's formula [56], where the thermal conductance per unit area is calculated as

$$h_{\text{NFRHT}} = \int_0^\infty \hbar\omega \frac{\partial f_{\text{BE}}}{\partial T} \left[\int_0^\infty \xi_{12}(\omega, k_{\parallel}) k_{\parallel} \frac{dk_{\parallel}}{2\pi} \right] \frac{d\omega}{2\pi}. \quad (9)$$

The integrand in Eq. (9) thus represents the spectral thermal conductance of NFRHT, and will be compared to that obtained from NEMD in the previous subsection.

The calculation of the photon tunneling probability $\xi_{12}(\omega, k_{\parallel})$ requires the knowledge of the local dielectric function of bulk MgO [2,56]. To ensure a consistent comparison between the present NEMD and the FE theory, we compute the dielectric function by EMD simulation using the same atomic interaction potential as in NEMD.

The local dielectric function tensor is related to the dielectric susceptibility $\chi_{\alpha\beta}(\omega)$ as [58,59] $\varepsilon_{\alpha\beta}(\omega) = \delta_{\alpha\beta} + \chi_{\alpha\beta}(\omega)$, with $\delta_{\alpha\beta}$ the Kronecker delta, and $\chi_{\alpha\beta}(\omega)$ calculated via the fluctuation-dissipation theorem (i.e. Green-Kubo formula [58–60]):

$$\chi_{\alpha\beta}(\omega) = \frac{V}{\varepsilon_0 k_B T} \left[\langle P_\alpha(0) P_\beta(0) \rangle + i\omega \int_0^\infty \exp(i\omega t) \langle P_\alpha(t) P_\beta(0) \rangle dt \right], \quad (10)$$

where V is the system volume and ε_0 is the vacuum permittivity. In Eq. (10), the polarization of the system is calculated as the density of dipole moment: $\mathbf{P}(t) = 1/V \sum_i e_i \mathbf{u}_i(t)$, with $\mathbf{u}_i = \mathbf{r}_i - \mathbf{r}_{i,0}$ the atomic displacement with respect to its equilibrium position $\mathbf{r}_{i,0}$. In the numerical implementation, we adopt a $10 \times 10 \times 10$ supercell of 8000 atoms in the EMD simulation with a time step of 0.5 fs. The size of the supercell has been tested to be sufficiently large to capture well the long-range interaction. First, 1×10^6 time steps are run under the *NVT* (canonical) ensemble for structure relaxation, after which 5×10^6 time steps are run under the *NVE* ensemble. The polarization of the system is output once per 20 time steps during the *NVE* run. Ten independent simulations are conducted to reduce the statistical fluctuations. As shown in Fig. 2, the local dielectric function calculated by EMD at 300 K generally agrees well with the available experimental data [57], similar to the findings in Ref. [49]. Note that the electronic degrees of freedom are not taken into account in the MD simulation, which only captures the ionic contribution to dielectric response as the dominant mechanism in the infrared regime. Following Ref. [59], in Fig. 2 we have included a constant correction term to account for the electronic contribution as $\varepsilon_{\alpha\beta}(\omega) = \delta_{\alpha\beta} + \chi_{\alpha\beta}(\omega) + (\varepsilon_\infty - 1)\delta_{\alpha\beta}$, with $\varepsilon_\infty = 3.01$ being the high-frequency dielectric constant [57].

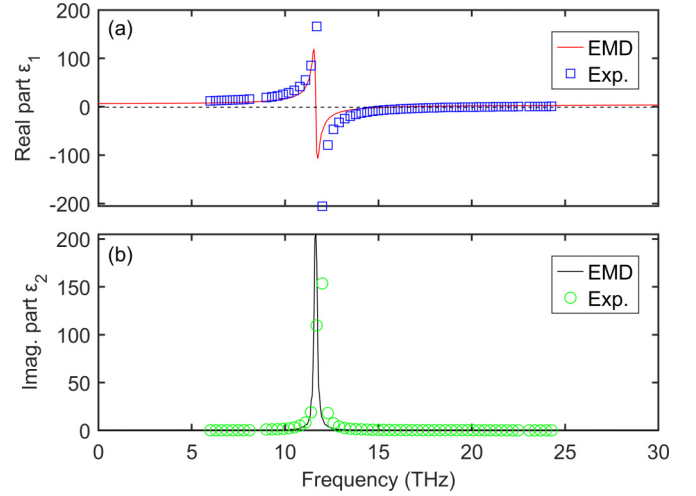


FIG. 2. Local dielectric function ($\varepsilon = \varepsilon_1 + i\varepsilon_2$) of bulk MgO at 300 K in infrared regime: (a) Real part (ε_1); (b) Imaginary (Imag.) part (ε_2). Discrete symbols represent experimental data from literature [57], whereas red and black solid lines denote present result calculated by equilibrium molecular dynamics. Black dashed line in (a) represents $\varepsilon_1 = -1$ corresponding to resonance frequency.

III. RESULTS AND DISCUSSION

In this section, we first present the results of the spectral and overall thermal conductance of MgO-MgO nanogap at 300 K in Sec. III A and Sec. III B, respectively. We also compare the NEMD results with the FE local theory to examine the validity of the latter. The role of lattice anharmonicity on heat transfer across the vacuum nanogap is finally discussed in Sec. III C.

A. Transmission function and spectral thermal conductance

The frequency-dependent transmission functions across three MgO-MgO nanogaps with a gap size of 6 Å, 1 nm, and 2 nm by NEMD at 300 K are shown in Fig. 3(a). To have an intuitive understanding of which phonon branch contributes to the heat tunneling, we calculate the phonon dispersion via the nonlocal dielectric function by EMD, as plotted in Fig. 3(b). The Γ - X direction is chosen corresponding to the $[1\ 0\ 0]$ transport direction. The frequency- and wave-vector dependent (i.e., nonlocal) dielectric function is related to the dielectric susceptibility as $\varepsilon_{\alpha\beta}(\omega, \mathbf{k}) = \varepsilon_\infty \delta_{\alpha\beta} + \chi_{\alpha\beta}(\omega, \mathbf{k})$, where $\chi_{\alpha\beta}(\omega, \mathbf{k})$ is calculated through a generalized version of the Green-Kubo formula in Eq. (10):

$$\chi_{\alpha\beta}(\omega, \mathbf{k}) = \frac{V}{\varepsilon_0 k_B T} \left[\langle P_\alpha^*(0, \mathbf{k}) P_\beta(0, \mathbf{k}) \rangle + i\omega \int_0^\infty \exp(i\omega t) \langle P_\alpha^*(t, \mathbf{k}) P_\beta(0, \mathbf{k}) \rangle dt \right], \quad (11)$$

with the superscript “*” denoting the complex conjugate. The wave-vector dependent polarization of the system is calculated by the following projection:

$$\mathbf{P}(t, \mathbf{k}) = \frac{1}{V} \sum_{l\kappa} e_{l\kappa} \mathbf{u}_{l\kappa}(t) \exp(i\mathbf{k} \cdot \mathbf{r}_{l,0}), \quad (12)$$

where the atomic index $l\kappa$ includes the indices of lattice unit cell (l) and atoms within one unit cell (κ), respectively, and

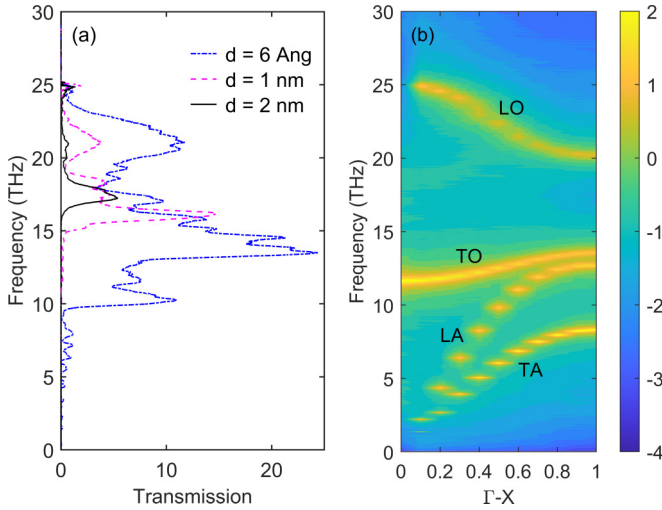


FIG. 3. Frequency-dependent (a) transmission function by NEMD of MgO-MgO nanogaps with gap size of 6 Å, 1 nm, and 2 nm, respectively, and (b) imaginary part of nonlocal dielectric function in log scale (i.e., $\log \varepsilon_2$) of bulk MgO showing phonon dispersion along Γ -X direction. System temperature is 300 K.

$r_{l,0}$ is the equilibrium position of lattice unit cell. The different phonon branches are clearly seen in Fig. 3(b), with the broadening from the anharmonic phonon-phonon scattering. The present way to compute the phonon dispersion from EMD is in principle equivalent to the classical spectral energy density analysis used to extract the phonon dispersion and lifetimes [61]. The nonlocal dielectric function could be also calculated via NEMD by imposing an external electric field and evaluating the induced polarization of the system [62]. However, the implementation is more tedious compared to the EMD based on the Green-Kubo formula here. In principle, the dielectric functions obtained by NEMD and EMD should be equivalent in the linear response regime, although a rigorous verification is beyond the scope of the present study.

As shown in Fig. 3(a), the transmission function is generally reduced in both spectral range and magnitude as the gap size increases. For gap size ≥ 1 nm, the transmission function is almost negligible at a frequency lower than 15 THz. In other words, only optical modes could go through those nanogaps, based on the phonon dispersion in Fig. 3(b). At a gap size of 6 Å, there is also energy transmission in the lower-frequency range corresponding to acoustic phonons. To be more specific, the significant peak around 10 THz shall be contributed by the longitudinal acoustic (LA) phonons, whereas the few small peaks between 5 ~ 10 THz could be due to both LA and transverse acoustic (TA) phonons.

As the validity of classical FE theory remains unclear in radiative heat transfer across few-nanometer polar dielectric vacuum gap [11,14], we examine this issue by using the NEMD results as benchmark. To be more specific, we make a comparison of the spectral thermal conductance by NEMD to that predicted by FE local theory, as shown in Fig. 4. For a fair comparison, the quantum-corrected thermal conductance by NEMD as calculated in Eq. (7) is used, whereas the electronic contribution to the dielectric function ($\varepsilon_\infty - 1$) is excluded in the FE theoretical calculation. There is only one peak in the

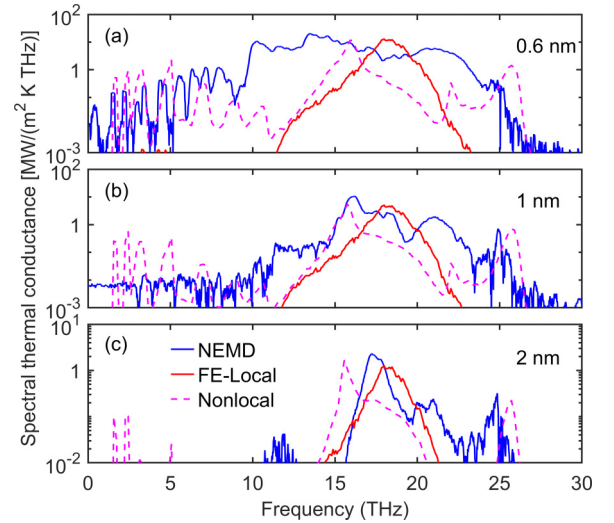


FIG. 4. Spectral thermal conductance of MgO-MgO nanogaps at gap size of (a) 0.6 nm, (b) 1 nm, and (c) 2 nm. Blue solid lines denote present quantum-corrected result by nonequilibrium molecular dynamics, whereas red solid lines denote result by fluctuational electrodynamics theory with local dielectric function calculated by EMD (cf. Fig. 2), and magenta dashed lines denote result by nonlocal theory for radiative heat transfer from Ref. [37].

thermal spectrum of NRFHT predicted by FE local theory. This resonance peak is known to be caused by the surface phonon polaritons from the hybridization of transverse optical (TO) phonons and electromagnetic waves [63]. The frequency of the resonance peak lies where the real part of the local dielectric function in Fig. 2 reaches -1 , which does not coincide with the frequency of TO phonons, whereas the broadening of the peak comes from anharmonic damping. At the smallest gap size of 6 Å in Fig. 4(a), a very broad thermal spectrum is obtained by NEMD, which shows a very large deviation from the FE local theory. This is clear evidence of the failure of the continuum FE theory with local dielectric response. As the gap size increases to 1 and 2 nm in Figs. 4(b) and 4(c), respectively, the difference between the results of NEMD and FE local theory tends to become gradually smaller. Actually, at the 2-nm gap, the thermal spectrum from NEMD shows a significant peak at ~ 17.5 THz that is quite close to the resonance peak predicted by FE theory. Note that the height of the second peak at ~ 25 THz is only $\sim 10\%$ of the height of the main peak. The results at 2 nm gap indicate that NEMD indeed captures the near-field heat transfer by electromagnetic waves between polar crystals. The underlying reason lies in the fact that the interatomic potential in Eq. (1) adequately includes the Coulomb interaction between ions, i.e., the ionic electrostatic interaction. Thus NEMD captures successfully the electrical fields generated by the vibrating charged ions, i.e., the evanescent waves or surface phonon polaritons, as already validated in a previous pioneering study [44]. As only electrostatics is considered, the present NEMD simulation is not able to describe the propagation of electromagnetic waves (i.e., the retardation effect), which is important in far-field radiative heat transfer yet negligible in the extreme near-field regime [2]. We have not simulated even larger nanogaps mainly due to two reasons: (i) the intensive

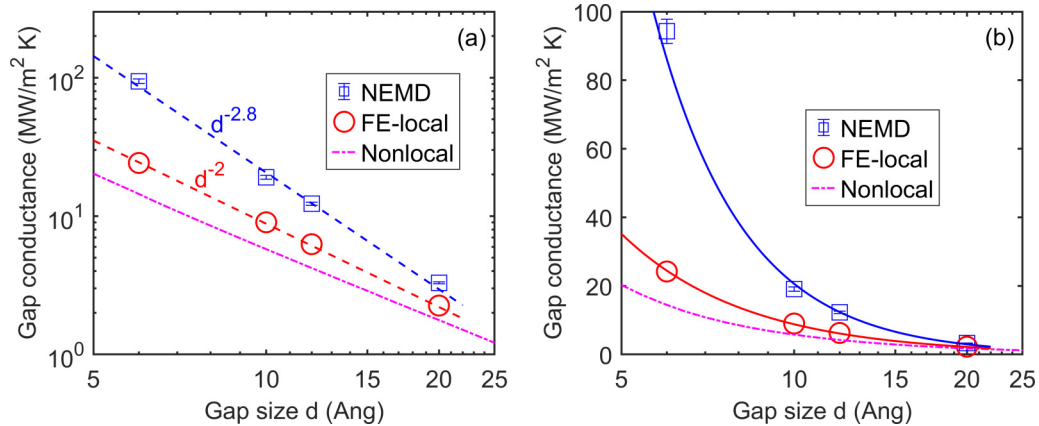


FIG. 5. Thermal conductance of MgO-MgO nanogaps vs gap size d at 300 K in (a) log-log scale and (b) log-normal scale. Blue squares with error bar denote present quantum-corrected results by NEMD, whereas red circles denote near-field radiative heat transfer result by FE theory using local dielectric function calculated by EMD (cf. Fig. 2), and magenta dashed-dotted lines denote result by nonlocal theory for radiative heat transfer from Ref. [37]. Solid lines in (b) are used for guiding the eye.

computational cost required to eliminate the size effect to accurately describe the slowly decaying long-range Coulomb forces, and (ii) the very large fluctuations of the NEMD conductance for large gaps.

The deviation between continuum theory and NEMD at very small gap size has two main origins: (i) the phonon tunneling due to direct short-range atomic interaction across the gap, similar to that in heat transport through metallic vacuum nanogaps [41], and (ii) the nonlocal dielectric response of polar materials from long-range interaction between dipole moments generated by ionic vibrations, including the optical response of both acoustic phonons [37] and longitudinal optical (LO) phonons [64]. The nonlocal dielectric response is highlighted in the frequency- and wave-vector dependent dielectric function shown in Fig. 3(b). In contrast to local dielectrics where only Γ -point TO phonons couple to the electromagnetic waves, all the branches including LO, TO, LA, and TA phonons throughout the Brillouin zone show clear optical response (i.e., infrared absorption). As a comparison, we include in Fig. 4 our recent result by nonlocal theory for radiative heat transfer at atomic scale [37]. Although a perfect agreement with nonlocal theory is not achieved, our NEMD simulation captures well some crucial features of nonlocal dielectric response predicted by the theory, especially the contribution from acoustic phonons at the smallest gap. It remains, however, a challenging task to disentangle the contributions from phonon tunneling and from nonlocal dielectric response in the present methodology.

B. Thermal conductance

The overall thermal conductance of MgO-MgO nanogap is obtained by integrating the spectral thermal conductance in Sec. III A over the whole frequency range, as given in Fig. 5(a) in log-log scale and in Fig. 5(b) in log-normal scale. In the current studied range of gap size from 6 Å to 2 nm, the thermal conductance across the gap by NEMD is higher than that of NFRHT predicted by FE local theory. The underlying reason is due to both phonon tunneling and nonlocal dielectric response, as discussed at the end of Sec. III A.

On the other hand, the NEMD result is gradually approaching that of FE theory as the gap size increases, with a faster decaying trend of $h \propto d^{-2.8}$ compared to $h \propto d^{-2}$ in the latter. There is still non-negligible difference between them at the 2-nm gap, while the convergence of NEMD to FE local theory is expected at larger gap size. A recent study [64] has estimated a nonlocal length of ~ 10 nm in polar dielectric materials, which indeed indicates appreciable nonlocal optical response at few-nanometer scale. This is caused by the slowly decaying Coulomb interaction, which also explains the much slower decay trend of the thermal conductance compared to that ($h \propto d^{-9}$) characterizing the metallic nanogaps [41]. In Fig. 5, we have also included the thermal conductance across the gap predicted by the nonlocal theory in our recent work [37]. In contrast to the NEMD conductance, the nonlocal theoretical result is lower than that by the FE local theory. Such a discrepancy needs to be investigated in depth in the future, since we are not able to disentangle the nonlocal dielectric response and phonon tunneling in this work. Note that in NEMD, the thermal conductance will not diverge as $h \propto d^{-2.8}$ when the gap size further decreases. Instead, a transition to the contact heat conduction should occur, as already shown in previous works [45,46]. Actually, when setting the gap size as half of the lattice constant of bulk MgO in NEMD simulation, we will recover exactly the heat conduction across a MgO film.

We would like to point out the importance of taking into account the anharmonicity in the comparison of atomistic simulation and continuum FE theory. In the lattice dynamics theory, the local dielectric function of simple ionic crystals like MgO is given by [65]

$$\varepsilon(\omega) = \varepsilon_{\infty} + \frac{S}{\Omega_{\text{TO}}^2(\omega) - \omega^2 - 2i\omega\Gamma(\omega)}, \quad (13)$$

where ω_{TO} is the eigenfrequency of TO phonon at 0 K, and $\Omega_{\text{TO}}(\omega) = \omega_{\text{TO}} + \Delta(\omega)$ is the renormalized eigenfrequency of TO phonon considering its frequency shift $\Delta(\omega)$, $\Gamma(\omega)$ is its damping resulting from anharmonic phonon-phonon scattering, and S is the oscillator strength. The imaginary part of the dielectric function in Eq. (13) is expressed as a

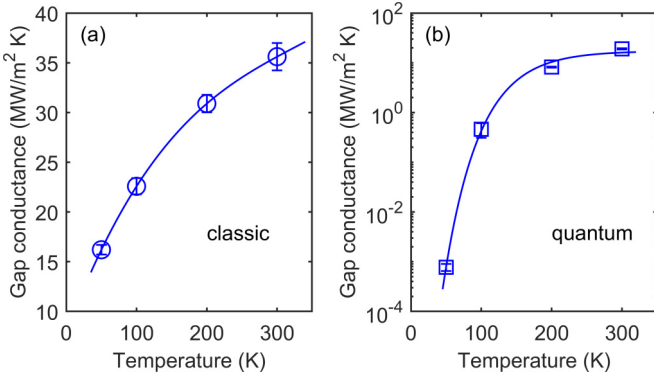


FIG. 6. Temperature-dependent thermal conductance of 1-nm MgO-MgO nanogap by NEMD: (a) classical conductance via Eq. (6), and (b) quantum-corrected conductance via Eq. (7). Solid lines are used for guiding the eye.

Lorentzian function:

$$\varepsilon_2(\omega) = \frac{2S\omega_{\text{TO}}\Gamma(\omega)}{[\Omega_{\text{TO}}^2(\omega) - \omega^2]^2 + 4\omega_{\text{TO}}^2\Gamma^2(\omega)}. \quad (14)$$

In the harmonic limit [$\Gamma(\omega) \rightarrow 0$], the imaginary part in Eq. (14) will be reduced to a Dirac delta function, which makes the calculation of NFRHT via Eq. (9) impractical. From this perspective, the comparison of harmonic NEGF to FE theory for heat transport across polar dielectric nanogaps in Ref. [46] remains debatable due to the inconsistency between the inputs of the atomic interaction forces. To be more specific, only harmonic forces are employed in the former, whereas both the harmonic and anharmonic forces are essential for calculating the dielectric function in the latter. In this work, our comparison is more consistent since the same atomic interaction is included in the NEMD and in the calculation of dielectric function as input into the continuum FE theory. The critical gap size (> 2 nm) where the continuum theory is recovered in the present work is larger than that (~ 1 nm) found in Ref. [46].

C. The role of anharmonicity

Finally, we investigate the role of anharmonicity on the extreme near-field heat transport across MgO-MgO nanogap, as motivated by the significant effect of the anharmonic phonon-phonon scattering on the dielectric response of polar materials. The 1-nm nanogap is considered, and we raise the strength of anharmonicity by varying the system temperature from 50 to 300 K. As shown in Fig. 6(a), the classical thermal conductance obtained by NEMD increases as the temperature rises, and its value at 300 K is more than twice that at 50 K. It has been known that the increase of thermal boundary conductance with temperature at solid-solid interface predicted by NEMD is attributed to the inelastic anharmonic phonon scattering [66]. Thus, the present temperature-dependent trend of thermal conductance across the gap is most likely caused by the lattice anharmonicity. As a comparison, the thermal conductance of metallic vacuum nanogaps in our previous study increases only ~ 20 – 30% from 1 to 300 K, which indicates moderate anharmonic effect [41]. According to Eq. (6), the increasing thermal conductance across the gap could only come

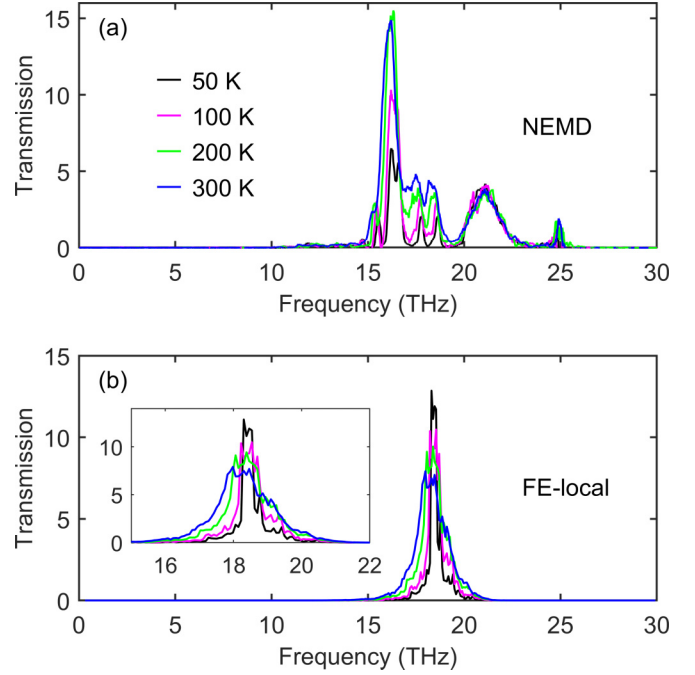


FIG. 7. Temperature-dependent transmission function across MgO-MgO nanogap with gap size of 1 nm: (a) NEMD result and (b) near-field radiative heat transfer result by FE theory with local dielectric function calculated by EMD (cf. Fig. 2). Inset in (b) shows enlarged plot between 15 and 22 THz.

from the enhanced energy transmission, since the spectral-heat capacity is a constant (k_B) in the classical limit. In Fig. 6(b), the quantum-corrected thermal conductance calculated via Eq. (7) varies by more than four orders of magnitude in the same temperature range, as mainly contributed by the increasing phonon population from Bose-Einstein statistics.

The enhanced energy transmission across the nanogap with increasing temperature is explicitly demonstrated in Fig. 7(a). Interestingly, the enhancement occurs mainly in the frequency range between 15 and 20 THz, while the transmission function is almost independent of temperature between 20 and 25 THz. As a comparison, we also plot the temperature-dependent transmission function of NFRHT predicted by the FE theory, i.e., the term in the square bracket of Eq. (9), as shown in Fig. 7(b). Here, the local dielectric functions at corresponding temperatures are computed by EMD and then used for FE theoretical calculation. As the temperature increases, the peak in the transmission function curve is reduced while it is broadened. This can be explained by the same trend of

TABLE III. Independence verification of cross-section size (in u.c.) in NEMD model of 1-nm MgO-MgO nanogap. $L_{\text{th}} = 5$ u.c., $L_r = L_d = 4$ u.c. Standard deviation of thermal conductance across gap is computed from five independent NEMD simulations.

Cross section (u.c. \times u.c.)	$h_{\text{NEMD}} (\times 10^7 \text{W/m}^2 \text{K})$
6×6	$3.82 (\pm 0.06)$
8×8	$3.83 (\pm 0.10)$
10×10	$3.93 (\pm 0.04)$

TABLE IV. Independence verification of size (in u.c.) of fixed layer and device region in molecular dynamics model of 1-nm MgO-MgO nanogap. $L_{\text{th}} = 5$ u.c., cross-section size: $8\text{u.c.} \times 8\text{u.c.}$ h_{SHC} is calculated by integrating spectral heat current (SHC) extracted from NEMD.

L_f (u.c.)	L_d (u.c.)	h_{NEMD} ($\times 10^7 \text{W/m}^2 \text{K}$)	h_{SHC} ($\times 10^7 \text{W/m}^2 \text{K}$)	$h_{\text{SHC}}/h_{\text{NEMD}}$ (%)
4	4	3.83 (± 0.10)	3.37 (± 0.13)	87.98
4	6	3.82 (± 0.05)	3.50 (± 0.12)	91.53
4	8	3.73 (± 0.08)	3.47 (± 0.06)	93.07
8	8	3.82 (± 0.08)	3.57 (± 0.07)	93.38
10	10	3.79 (± 0.08)	3.58 (± 0.15)	94.41
12	12	3.75 (± 0.11)	3.56 (± 0.14)	95.01

local dielectric function in Eq. (14) since the damping (i.e., the phonon linewidth) increases with temperature. However, the trend is quite different in the result by NEMD, namely, the peaks are enhanced and also broadened between 15 and 20 THz. It could not be explained by the effect of anharmonicity on the local dielectric response of the material. The impact of anharmonic phonon scattering on either the nonlocal response or the phonon tunneling may be one possible reason, which remains to be further investigated in future works.

IV. CONCLUSIONS

In summary, we present an atomistic modeling of the extreme near-field heat transport across polar dielectric vacuum nanogaps. At angstrom- and nanometer-sized gaps, the direct non-equilibrium molecular dynamics result shows significant deviations from the continuum fluctuational electrodynamics theory with consistent microscopic input, due to both phonon tunneling and nonlocal dielectric response. The NEMD results gradually approach that of the continuum theory and are expected to recover the latter at larger nanogaps. The energy transmission across the nanogap increases as the temperature rises, attributed to the effect of lattice anharmonicity. Our results highlight the importance of nonlocal effects stemming from both acoustic and optical phonons in the extreme near-field regime. The atomistic simulation allows one to take into account all contributions to the energy transfer. However, to date we are not able to quantify the relative contribution of the tunneling of phonons with respect to their radiative contribution. This analysis will be the subject of a future work.

ACKNOWLEDGMENTS

This work was supported by the French Agence Nationale de la Recherche (ANR), under Grant No. ANR-20-CE05-0021-01 (NearHeat). Y.G. would like to thank Dr. S. Volz for his helpful discussions about the microscopic picture of near-field heat transfer, and also appreciates the financial support of the starting-up funding (Grant No. AUGA2160500923)

from Harbin Institute of Technology and the NSFC Fund for Excellent Young Scientists Fund Program (Overseas). The simulation used the computational resources of Raptor of iLM at the Université Claude Bernard Lyon 1.

APPENDIX: SIZE-INDEPENDENCE VERIFICATION OF NEMD MODEL

Here, we provide the details of size-independence verification of the dimension of NEMD model for the 1-nm MgO nanogap as an example. First, we verify the influence of cross-section size by fixing $L_{\text{th}} = 5$ u.c., $L_f = L_d = 4$ u.c. As the cross section increases from $6\text{u.c.} \times 6\text{u.c.}$ to $10\text{u.c.} \times 10\text{u.c.}$, the classical thermal conductance directly obtained by NEMD increases less than 3%, as summarized in Table III. Thus, we adopt a cross section of $8\text{u.c.} \times 8\text{u.c.}$ for the NEMD simulation of 1-nm gap.

We further verify the influence of the size of the fixed layer (L_f) and the device region ($2L_d$) at $L_{\text{th}} = 5$ u.c. using a cross section of $8\text{u.c.} \times 8\text{u.c.}$ As L_f and L_d increase, the classical thermal conductance directly obtained by NEMD (h_{NEMD}) almost does not change, as shown in Table IV. In contrast, the classical thermal conductance obtained by integrating the spectral heat current from NEMD (h_{SHC}), i.e., based on Eq. (6), gradually increases and approaches that directly obtained by NEMD. We have a small mismatch between h_{SHC} and h_{NEMD} since the spectral heat current is calculated between the left-hand side and right-hand side of the device region. Due to the long-range Coulomb interaction, there is some heat flow between the left-hand (right-hand) thermostat and right-hand (left-hand) side of the device region. To avoid such spurious effect and considering the periodic boundary condition along the transport direction, we increase L_f and L_d to be sufficiently large such that difference between h_{SHC} and h_{NEMD} is less than 5%, i.e., within the statistical uncertainty of NEMD simulation, as summarized in Table IV. Finally, we adopt $L_f = L_d = 12$ u.c. for the NEMD simulation of 1-nm gap.

- [1] A. Volokitin and B. N. Persson, *Rev. Mod. Phys.* **79**, 1291 (2007).
- [2] Z. M. Zhang, *Nano/Microscale Heat Transfer* (McGraw-Hill, New York, 2007).
- [3] S. M. Rytov, Y. A. Kravtsov, and V. I. Tatarskii, *Principles of Statistical Radiophysics 3* (Springer, Heidelberg, 1989).
- [4] C. Hargreaves, *Phys. Lett. A* **30**, 491 (1969).

- [5] A. Narayanaswamy, S. Shen, and G. Chen, *Phys. Rev. B* **78**, 115303 (2008).
- [6] S. Shen, A. Narayanaswamy, and G. Chen, *Nano Lett.* **9**, 2909 (2009).
- [7] E. Rousseau, A. Siria, G. Jourdan, S. Volz, F. Comin, J. Chevrier, and J.-J. Greffet, *Nat. Photonics* **3**, 514 (2009).

- [8] R. Ottens, V. Quetschke, S. Wise, A. Alemi, R. Lundock, G. Mueller, D. H. Reitze, D. B. Tanner, and B. F. Whiting, *Phys. Rev. Lett.* **107**, 014301 (2011).
- [9] T. Kralik, P. Hanzelka, M. Zobac, V. Musilova, T. Fort, and M. Horak, *Phys. Rev. Lett.* **109**, 224302 (2012).
- [10] B. Song, Y. Ganjeh, S. Sadat, D. Thompson, A. Fiorino, V. Fernández-Hurtado, J. Feist, F. J. García-Vidal, J. C. Cuevas, and P. Reddy, *Nat. Nanotechnol.* **10**, 253 (2015).
- [11] K. Kim, B. Song, V. Fernández-Hurtado, W. Lee, W. Jeong, L. Cui, D. Thompson, J. Feist, M. H. Reid, F. J. García-Vidal, J. C. Cuevas, E. Meyhofer, and P. Reddy, *Nature (London)* **528**, 387 (2015).
- [12] R. St-Gelais, L. Zhu, S. Fan, and M. Lipson, *Nat. Nanotechnol.* **11**, 515 (2016).
- [13] M. Ghashami, H. Geng, T. Kim, N. Iacopino, S. K. Cho, and K. Park, *Phys. Rev. Lett.* **120**, 175901 (2018).
- [14] H. Salihoglu, W. Nam, L. Traverso, M. Segovia, P. K. Venuthurumilli, W. Liu, Y. Wei, W. Li, and X. Xu, *Nano Lett.* **20**, 6091 (2020).
- [15] A. Kittel, W. Müller-Hirsch, J. Parisi, S.-A. Biehs, D. Reddig, and M. Holthaus, *Phys. Rev. Lett.* **95**, 224301 (2005).
- [16] L. Worbes, D. Hellmann, and A. Kittel, *Phys. Rev. Lett.* **110**, 134302 (2013).
- [17] K. Kloppstech, N. Köne, S.-A. Biehs, A. W. Rodriguez, L. Worbes, D. Hellmann, and A. Kittel, *Nat. Commun.* **8**, 14475 (2017).
- [18] L. Cui, W. Jeong, V. Fernández-Hurtado, J. Feist, F. J. García-Vidal, J. C. Cuevas, E. Meyhofer, and P. Reddy, *Nat. Commun.* **8**, 14479 (2017).
- [19] A. Jarzembki, T. Tokunaga, J. Crossley, J. Yun, C. Shaskey, R. A. Murdick, I. Park, M. Francoeur, and K. Park, *Phys. Rev. B* **106**, 205418 (2022).
- [20] Y. De Wilde, F. Formanek, R. Carminati, B. Gralak, P.-A. Lemoine, K. Joulain, J.-P. Mulet, Y. Chen, and J.-J. Greffet, *Nature (London)* **444**, 740 (2006).
- [21] I. Altfeder, A. A. Voevodin, and A. K. Roy, *Phys. Rev. Lett.* **105**, 166101 (2010).
- [22] A. C. Jones and M. B. Raschke, *Nano Lett.* **12**, 1475 (2012).
- [23] M. H. Kryder, E. C. Gage, T. W. McDaniel, W. A. Challener, R. E. Rottmayer, G. Ju, Y.-T. Hsia, and M. F. Erden, *Proc. IEEE* **96**, 1810 (2008).
- [24] W. Challener, C. Peng, A. Itagi, D. Karns, W. Peng, Y. Peng, X. Yang, X. Zhu, N. Gokemeijer, and Y.-T. Hsia, *Nat. Photonics* **3**, 220 (2009).
- [25] B. C. Stipe, T. C. Strand, C. C. Poon, H. Balamane, T. D. Boone, J. A. Katine, J.-L. Li, V. Rawat, H. Nemoto, and A. Hirotsune, *Nat. Photonics* **4**, 484 (2010).
- [26] W. Srituravanich, N. Fang, C. Sun, Q. Luo, and X. Zhang, *Nano Lett.* **4**, 1085 (2004).
- [27] M. Lee, R. L. Vink, C. A. Volkert, and M. Krüger, *Phys. Rev. B* **104**, 174309 (2021).
- [28] A. Volokitin, *Appl. Surface Sci. Adv.* **6**, 100160 (2021).
- [29] M. Prunnila and J. Meltaus, *Phys. Rev. Lett.* **105**, 125501 (2010).
- [30] Y. Ezzahri and K. Joulain, *Phys. Rev. B* **90**, 115433 (2014).
- [31] J. Pendry, K. Sasihihlu, and R. Craster, *Phys. Rev. B* **94**, 075414 (2016).
- [32] Z. Geng and I. J. Maasilta, *Phys. Rev. Res.* **4**, 033073 (2022).
- [33] E. L. Wolf, *Principles of Electron Tunneling Spectroscopy* (Oxford University Press, 2012).
- [34] Z.-Q. Zhang, J.-T. Lü, and J.-S. Wang, *Phys. Rev. B* **97**, 195450 (2018).
- [35] M. Gómez Vitoria, Y. Guo, S. Merabia, P. Ben-Abdallah, and R. Messina, *Phys. Rev. B* **107**, 125414 (2023).
- [36] P.-O. Chapuis, S. Volz, C. Henkel, K. Joulain, and J.-J. Greffet, *Phys. Rev. B* **77**, 035431 (2008).
- [37] M. Gómez Vitoria, Y. Guo, S. Merabia, R. Messina, and P. Ben-Abdallah, *arXiv:2302.00520* (2023).
- [38] A. Alkurdi, C. Adessi, F. Tabatabaei, S. Li, K. Termentzidis, and S. Merabia, *Int. J. Heat Mass Transfer* **158**, 119963 (2020).
- [39] T. Tokunaga, A. Jarzembki, T. Shiga, K. Park, and M. Francoeur, *Phys. Rev. B* **104**, 125404 (2021).
- [40] W. Chen and G. Nagayama, *Int. J. Heat Mass Transfer* **176**, 121431 (2021).
- [41] Y. Guo, C. Adessi, M. Cobian, and S. Merabia, *Phys. Rev. B* **106**, 085403 (2022).
- [42] D. P. Sellan, E. Landry, K. Sasihihlu, A. Narayanaswamy, A. McGaughey, and C. Amon, *Phys. Rev. B* **85**, 024118 (2012).
- [43] T. Tokunaga, M. Arai, K. Kobayashi, W. Hayami, S. Suehara, T. Shiga, K. Park, and M. Francoeur, *Phys. Rev. B* **105**, 045410 (2022).
- [44] G. Domingues, S. Volz, K. Joulain, and J.-J. Greffet, *Phys. Rev. Lett.* **94**, 085901 (2005).
- [45] S. Xiong, K. Yang, Y. A. Kosevich, Y. Chalopin, R. D'Agosta, P. Cortona, and S. Volz, *Phys. Rev. Lett.* **112**, 114301 (2014).
- [46] V. Chiloyan, J. Garg, K. Esfarjani, and G. Chen, *Nat. Commun.* **6**, 6755 (2015).
- [47] M. Matsui, *J. Chem. Phys.* **91**, 489 (1989).
- [48] A. P. Thompson, H. M. Aktulga, R. Berger, D. S. Bolintineanu, W. M. Brown, P. S. Crozier, P. J. in't Veld, A. Kohlmeyer, S. G. Moore, and T. D. Nguyen, *Comput. Phys. Commun.* **171**, 108171 (2022).
- [49] Y. Chalopin, M. Hayoun, S. Volz, and H. Dammak, *Appl. Phys. Lett.* **104**, 011905 (2014).
- [50] M. P. Allen and D. J. Tildesley, *Computer Simulation of Liquids* (Oxford University Press, 2017).
- [51] K. Säskilahti, J. Oksanen, J. Tulkki, and S. Volz, *Phys. Rev. B* **90**, 134312 (2014).
- [52] K. Säskilahti, J. Oksanen, S. Volz, and J. Tulkki, *Phys. Rev. B* **91**, 115426 (2015).
- [53] K. Säskilahti, J. Oksanen, J. Tulkki, and S. Volz, *Phys. Rev. E* **93**, 052141 (2016).
- [54] A. Giri, J. L. Braun, and P. E. Hopkins, *J. Phys. Chem. C* **120**, 24847 (2016).
- [55] C. A. Polanco and L. Lindsay, *Phys. Rev. B* **99**, 075202 (2019).
- [56] S.-A. Biehs, E. Rousseau, and J.-J. Greffet, *Phys. Rev. Lett.* **105**, 234301 (2010).
- [57] E. D. Palik, *Handbook of Optical Constants of Solids* (Academic Press, San Diego, 1998), Vol. II.
- [58] A. Maradudin and R. J. P. R. Wallis, *Phys. Rev.* **123**, 777 (1961).
- [59] F. Gangemi, A. Carati, L. Galgani, R. Gangemi, and A. Maiocchi, *Europhys. Lett.* **110**, 47003 (2015).
- [60] W. Chen and L.-S. Li, *J. Appl. Phys.* **129**, 244104 (2021).
- [61] J. A. Thomas, J. E. Turney, R. M. Iutzi, C. H. Amon, and A. J. McGaughey, *Phys. Rev. B* **81**, 081411 (2010).
- [62] A. Mattoni and C. Caddeo, *J. Chem. Phys.* **152**, 104705 (2020).

- [63] J.-P. Mulet, K. Joulain, R. Carminati, and J.-J. Greffet, [Microscale Thermophys. Eng.](#) **6**, 209 (2002).
- [64] C. R. Gubbin and S. De Liberato, [Phys. Rev. X](#) **10**, 021027 (2020).
- [65] P. Brüesch, *Phonons: Theory and Experiments II* (Springer, Heidelberg, 1986).
- [66] R. J. Stevens, L. V. Zhigilei, and P. M. Norris, [Int. J. Heat Mass Transfer](#) **50**, 3977 (2007).